NAVAL AIR WARFARE CENTER AIRCRAFT DIVISION
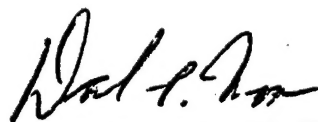**PATUXENT RIVER, MARYLAND**

TECHNICAL REPORT

REPORT NO: NAWCADPAX/TR-2004/12

EVOLUTION OF FRACTOGRAPH DURING FATIGUE AND STRESS CORROSION CRACKING

by

E. U. Lee
C. Lei
H. C. Sanders
R. Taylor

23 February 2004

20040303 192

DEPARTMENT OF THE NAVY
NAVAL AIR WARFARE CENTER AIRCRAFT DIVISION
PATUXENT RIVER, MARYLAND

EVOLUTION OF FRACTOGRAPH DURING FATIGUE AND STRESS CORROSION CRACKING

by

E. U. Lee
C. Lei
H. C. Sanders
R. Taylor

RELEASED BY:

_____ 23 Feb 2004

DALE MOORE / AIR-4.3.4 / DATE
Head, Materials Competency
Naval Air Warfare Center Aircraft Division

REPORT DOCUMENTATION PAGE		Form Approved OMB No. 0704-0188

Public reporting burden for this collection of information is estimated to average 1 hour per response, including the time for reviewing instructions, searching existing data sources, gathering and maintaining the data needed, and completing and reviewing this collection of information. Send comments regarding this burden estimate or any other aspect of this collection of information, including suggestions for reducing this burden, to Department of Defense, Washington Headquarters Services, Directorate for Information Operations and Reports (0704-0188), 1215 Jefferson Davis Highway, Suite 1204, Arlington, VA 22202-4302. Respondents should be aware that notwithstanding any other provision of law, no person shall be subject to any penalty for failing to comply with a collection of information if it does not display a currently valid OMB control number. **PLEASE DO NOT RETURN YOUR FORM TO THE ABOVE ADDRESS.**

1. REPORT DATE	2. REPORT TYPE	3. DATES COVERED
23 February 2004	Technical Report	

4. TITLE AND SUBTITLE	5a. CONTRACT NUMBER
Evolution of Fractograph during Fatigue and Stress Corrosion Cracking	5b. GRANT NUMBER
	5c. PROGRAM ELEMENT NUMBER

6. AUTHOR(S)	5d. PROJECT NUMBER
E. U. Lee H. C. Sanders	5e. TASK NUMBER
C. Lei R. Taylor	5f. WORK UNIT NUMBER

7. PERFORMING ORGANIZATION NAME(S) AND ADDRESS(ES)	8. PERFORMING ORGANIZATION REPORT NUMBER
Naval Air Warfare Center Aircraft Division 22347 Cedar Point Road, Unit #6 Patuxent River, Maryland 20670-1161	NAWCADPAX/TR-2004/12

9. SPONSORING/MONITORING AGENCY NAME(S) AND ADDRESS(ES)	10. SPONSOR/MONITOR'S ACRONYM(S)
Naval Air Systems Command 47123 Buse Road Unit IPT Patuxent River, Maryland 20670-1547	11. SPONSOR/MONITOR'S REPORT NUMBER(S)

12. DISTRIBUTION/AVAILABILITY STATEMENT

Approved for public release; distribution is unlimited.

13. SUPPLEMENTARY NOTES

14. ABSTRACT

Fatigue and stress corrosion cracking (SCC) behaviors were studied for three landing gear steels, AerMet 100, 300M, and 4340. The three steels were subjected to identical fatigue tests in vacuum, air, and 3.5% NaCl solution and identical stress corrosion cracking tests in 3.5% NaCl solution. The variation of fatigue crack growth rate with stress intensity range and maximum stress intensity was evaluated for different stress ratios and environments. Also, the variation of SCC rate with stress intensity was investigated. Subsequently, the fatigue- and SCC-induced crack surface morphologies were examined, and the fractographic evolution was defined with respect to the stress ratio, crack growth rate, stress intensity, and environment.

15. SUBJECT TERMS

Fatigue, Stress Corrosion Cracking, Crack Growth Rate, Environment, Stress Intensity Range, Stress Ratio, Fractograph

16. SECURITY CLASSIFICATION OF:			17. LIMITATION OF ABSTRACT	18. NUMBER OF PAGES	19a. NAME OF RESPONSIBLE PERSON E. U. Lee
a. REPORT	b. ABSTRACT	c. THIS PAGE			19b. TELEPHONE NUMBER (include area code)
Unclassified	Unclassified	Unclassified	SAR	44	(301) 342-8069

Standard Form 298 (Rev. 8-98)
Prescribed by ANSI Std. Z39-18

SUMMARY

The effects of stress ratio and environment on fatigue crack growth in AerMet 100, 300M, and 4340 steels were investigated. The employed stress ratios were 0.1 and 0.9, and the environments were vacuum, air, and 3.5% NaCl solution. In addition, the Stress Corrosion Cracking (SCC) behavior in 3.5% NaCl solution was studied to find the crack growth rate and threshold stress intensity. Then, the fatigue- and SCC-induced crack surface morphologies were examined with the aid of a scanning electron microscope. The change in fractographic features with stress ratio, crack growth rate, stress intensity, and environment was characterized, and the fractographic evolution was established.

Contents

ACKNOWLEDGEMENT

INTRODUCTION

Aircraft landing gear and other fracture critical components demand strong and tough materials to achieve high performance and great reliability. For such components, 4340, 300M, and AerMet 100 steels have been widely used. 4340 steel, developed in the 1940's, is a low alloy steel with good hardenability because of its appreciable content of C, Ni, Cr, and Mo. Its quench and temper heat treatment can induce high strength uniformly over a wide range of section sizes. This characteristic makes the steel attractive for many applications at -129 to $482°C$ (-200 to $900°F$), particularly in heavy sections. Some of the current applications include aircraft landing gear, gear, pinion, crankshaft, piston rod, and fastener. In the 1950's, this steel was modified to 300M steel, having somewhat higher strength along with better toughness. The modification, consisting of increasing contents of Si and Mo, improved the hardenability and resistance to softening during tempering. Its typical applications include aircraft landing gear, airframe part, fastener, gear, and shaft. However, its fracture toughness K_{IC} is only 57 MPa$\sqrt{m}$ (52 ksi$\sqrt{in}$.), which is not sufficient for fracture critical components, and a need of a steel with better damage tolerance and reliability was arisen. A new steel, designated as AF1410, was developed to have a higher $K_{IC} = 181$ MPa$\sqrt{m}$ (165 ksi$\sqrt{in}$.) (reference 1). This steel, however, left much to be desired with regard to tensile strength. Its ultimate tensile strength is only 1,669 MPa (242 ksi), which is not suitable for highly stressed structural components, requiring high strength to weight ratio. In the early 1990's, a new Co-Ni alloy steel, strengthened with C, Cr, and Mo, AerMet 100 steel, was developed (reference 2). It has an outstanding combination of high ultimate tensile strength, 1,979 MPa (287 ksi), and high K_{IC}, exceeding 110 MPa$\sqrt{m}$ (100 ksi$\sqrt{in}$.). Therefore, AerMet 100 steel has been used more and more for aircraft components, such as landing gear, arresting gear shank, horizontal stabilizer spindle, wingfold transmission, and wing pivot pin.

Although the mechanical and metallurgical properties have been improved much, the three steels, AerMet 100, 300M, and 4340, are still susceptible to cracking under static and repetitive loading. Determining the cause of cracking is vital in preventing a recurrence. One of the most important sources of information relating to the cracking is the crack surface itself. A crack surface morphology is a detailed record of the cracking history and contains the evidence of loading history, environmental effect, and material quality. The objective of this study is to characterize the fatigue and Stress Corrosion Cracking (SCC) behaviors of the three steels and clarify the related crack surface morphology or fractograph. Furthermore, it attempts to understand the evolution of fractograph in inert and corrosive environments and establish the cracking mechanisms in respective environments.

EXPERIMENTAL PROCEDURE

MATERIAL AND SPECIMEN

As the specimen materials, slabs of AerMet 100, 300M, and 4340 steels were used. Their nominal chemical compositions are shown in table 1.

Table 1: Chemical Composition (wt %) of Three Steels

Element	AerMet 100	300M	4340
C	0.23	0.38~0.43	0.38~0.43
Mn	0.03	0.60~0.90	0.60~0.90
Si	0.03	1.45~1.80	0.15~0.35
P	0.003	~ 0.010	~ 0.015
S	0.0009	~ 0.010	~ 0.015
Cr	3.03	0.70~0.95	0.70~0.90
Ni	11.09	1.65~2.00	1.65~2.00
Mo	1.18	0.30~0.50	0.20~0.30
Cu	0.01	~ 0.35	-
Co	13.44	-	-
Fe	Balance	Balance	Balance

These slabs were subjected to the following heat treatments, respectively.

AerMet 100 steel: preheating at 593°C (1,100°F) for 1.25 hr in vacuum, solution treating at 885°C (1,625°F) for 1.25 hr in vacuum and cooling in nitrogen atmosphere, freezing in dry-ice and alcohol (-73°C or –99°F) for 2 hr, and aging at 482°C (900°F) for 5 hr in air.

300M steel: solution treating at 871°C (1,600°F) for 5 hr in vacuum, oil quenching to below 71°C (160°F), and double tempering at 301°C (575°F) for 2 hr in vacuum.

4340 steel: solution treating at 843°C (1,550°F) for 1 hr, oil quenching to about 66°C (150°F), tempering at 232°C (450°F) for 3 hr, and air cooling.

The postheat treatment mechanical properties of the three steels are shown in table 2.

Table 2: Mechanical Properties of Three Steels

Property	AerMet 100	300M	4340
YS (Mpa)	1,724	1,703	1,669
UTS (Mpa)	1,979	2,000	1,944
KIC (MPa√m)	126	57	53

After the heat treatment, the microstructure of each steel was examined with an optical microscope. Subsequently, the slabs were machined to compact tension specimens, 38.1 mm (1.5 in.) wide and 4.8 mm (3/16 in.) thick, in the L-T crack plane orientation, employing an electro discharge machine. Before the fatigue and SCC tests, the specimen was precracked under constant amplitude loading of frequency 10 Hz at the test stress ratio of 0.1 or 0.9 in the test environment, vacuum, air, or 3.5% NaCl solution.

FATIGUE TEST

Two closed-loop servo-hydraulic mechanical test machines were used for the fatigue test. One was a 490 KN vertical Materials Testing System (MTS) machine for the fatigue test in vacuum and air and the other a 45 KN horizontal test machine for the fatigue test in liquid. The fatigue test was conducted under stress control in tension-tension cycling of frequency 10 Hz with a sinusoidal waveform and stress ratios, 0.1 and 0.9, in vacuum of 2×10^{-8} torr, air of 60% relative humidity, and 3.5% NaCl solution of pH 7.3 at room temperature. The fatigue loading procedure was K-decreasing or load shedding with K-gradient parameter $C = -0.08$ mm^{-1} (-2 in.$^{-1}$) in the near-threshold fatigue crack growth regime (Regime A) and K-increasing in the Paris and rapid unstable crack growth regimes (Regimes B and C). Using compliance technique, the fatigue crack length was continuously monitored with a laboratory computer system, interfaced with the MTS machine.

STRESS CORROSION CRACKING TEST

Two test methods were employed. One was Static Loading Test for the determination of crack growth rate da/dt and examination of fractograph at the final stage of SCC, and the other was Four-Point Bending Test for the examination of fractograph at the initial stage of SCC.

STATIC LOADING TEST WITH C(T) SPECIMEN

Before the test, a wedge was inserted into the notch of a precracked C(T) specimen to make a displacement, measurable with a clip-on displacement gage. Then, the crack tip was dipped in 3.5% NaCl solution of pH 7.3, and the crack length was measured with a binocular microscope, less frequently as the crack grew. The test was continued with crack length increasing and stress intensity, K_I, decreasing, and the threshold stress intensity for SCC, K_{ISCC}, was defined as the K_I at crack arrest. The K_I was calculated with the following equations (references 3 and 4).

$$K_I = (P/B\sqrt{W})[(2 + \alpha)/(1 - \alpha)^{3/2}](0.886 + 4.64\alpha - 13.32\alpha^2 + 14.72\alpha^3 - 5.6\alpha^4) \qquad (1)$$

$$BEV_o/P = [1 + (0.25/\alpha)][(1 + \alpha)/(1 - \alpha)]^2[1.61369 + 12.6778\alpha - 14.2311\alpha^2 - 16.6102\alpha^3 + 35.0499\alpha^4 - 14.4943\alpha^5] \qquad (2)$$

where P is the load, B the specimen thickness, W the specimen width, $\alpha = a/W$, a the crack length, E the modulus of elasticity, and V_o the displacement at front face of specimen. The data were reduced to crack length, a, versus time, t, and crack growth rate, da/dt, versus K_I plots.

FOUR-POINT BENDING TEST WITH NOTCHED SQUARE BAR SPECIMEN

The specimen was a square bar specimen of 10 x 10 x 70 mm with a Charpy notch at the mid-length. It was precracked to ½ thickness under cyclic three-point bending in air, and then step-loaded in four-point bending under constant displacement control in 3.5% NaCl solution of pH 7.3 without applying any external potential. The load was increased at 2% of the ultimate

bending strength each hour until the load drops, corresponding to the threshold crack growth or the initial stage of SCC. The K_I was calculated, using the following equation (reference 5).

$$K_I = \sigma\sqrt{\pi a}*F(\alpha) \tag{3}$$

$$F(\alpha) = 1.122 - 1.40\alpha + 7.33\alpha^2 - 13.08\alpha^3 + 14.0\alpha^4 \tag{4}$$

where σ is the gross stress $= 6M/BW^2$, M the bending moment $= Px$, and x the moment arm length.

FRACTOGRAPHY

For the fatigue test, the crack surface morphology was examined at several sites, corresponding to various crack growth rates, employing a scanning electron microscope, JEOL JSM-5800LV, operating at an accelerating voltage of 20 kV.

Since the Static Loading Test of SCC took many days and most of the crack surface was corroded severely in 3.5% NaCl solution, the fractographic examination was done only for the later stage of SCC with little corrosion. The fractographic examination for the initial stage of SCC was done with the Four-Point Bending Test specimen, which was corroded little.

RESULTS

MICROSTRUCTURE

The optical micrographs of the three steels exhibit tempered martensite, figure A-1. The diameters of prior austenite grain are 6 μm for the AerMet 100 steel, 14 μm for the 4340 steel, and 20 μm for the 300M steel.

VARIATION OF FATIGUE CRACK GROWTH/CYCLE, da/dN, WITH STRESS INTENSITY RANGE, ΔK

A sketch of typical da/dN versus ΔK curve with three regimes of fatigue crack growth is shown in figure A-2. This report follows the Suresh's regime designation of A for the near-threshold crack growth regime, B for the Paris regime, and C for the rapid unstable crack growth regime (reference 6).

STRESS RATIO EFFECT

Figure A-3 shows the da/dN versus ΔK curves, indicating the stress ratio effect, for the three steels. Raising stress ratio, R, from 0.1 to 0.9, moves the da/dN versus ΔK curve to the left, increasing the da/dN and reducing the threshold stress intensity range for fatigue crack growth, ΔK_{th}. At R = 0.9 in 3.5% NaCl solution, the curve levels off or da/dN is independent of ΔK in a region of ΔK.

ENVIRONMENTAL EFFECT

Figure A-4 indicates the environmental effect on the da/dN variation with ΔK for the three steels. (1) AerMet 100 steel: At R = 0.1, in Regime A, the da/dN is greater in air than in 3.5% NaCl solution and vacuum, and it is similar in the latter two environments. In Regime B, the da/dN is still greater in air, intermediate in 3.5% NaCl solution, and least in vacuum. In Regime C, the da/dN is similar in air and 3.5% NaCl solution, but it is greater than that in vacuum. At R = 0.9, in Regime A, the da/dN is greatest in 3.5% NaCl solution, intermediate in air, and smallest in vacuum. In Regime B, the da/dN curve levels off in 3.5% NaCl solution and crosses over the da/dN curve in air, and it is lower in vacuum. In Regime C, the three da/dN versus ΔK curves tend to converge. (2) 300M steel: At R = 0.1, in Regime A, the da/dN is slightly greater in 3.5% NaCl solution than in air. However, it is similar in Regimes B and C in air and 3.5% NaCl solution. The da/dN is lowest in vacuum in Regimes A and B. The three da/dN versus ΔK curves merge in Regime C. At R = 0.9, the da/dN is greatest in 3.5% NaCl solution, intermediate in air, and least in vacuum in Regimes A and B. The da/dN versus ΔK curve levels off in 3.5% NaCl solution, and the curves merge in Regime C in air and vacuum. (3) 4340 steel: The main features of da/dN variation with ΔK are similar to those for the 300M steel in the respective environments.

FATIGUE CRACK GROWTH RESISTANCES OF THREE STEELS

Figure A-5 compares the resistances of the three steels to fatigue crack growth, indicated by da/dN, in the three environments. (1) Vacuum: At R = 0.1, in Regime A, da/dN is greatest for 300M steel, intermediate for AerMet 100 steel, and least for 4340 steel. In Regime B, da/dN is similar for 300M and AerMet 100 steel and lowest for 4340 steel. In Regime C, the three curves tend to merge. At R = 0.9, in Regime A, the three da/dN versus ΔK curves overlap each other. In Regimes B and C, da/dN is similar for 300M and 4340 steels, whereas that of AerMet 100 steel is least. (2) Air: At R = 0.1, in Regime A, da/dN is greatest for 4340 steel, intermediate for 300M steel, and least for AerMet 100 steel. However, in Regimes B and C, the three da/dN versus ΔK curves overlap each other, indicating similar da/dN. At R = 0.9, in Regime A, the three da/dN versus ΔK curves nearly overlap each other. In Regimes B and C, the da/dN versus ΔK curves of 300M and 4340 steels nearly overlap each other, and da/dN is lowest for AerMet 100 steel. (3) 3.5% NaCl solution: Throughout the three regimes, da/dN is greatest for 4340 steel, intermediate for 300M steel, and least for AerMet 100 steel, except the da/dN for 300M steel is partly close to those for 4340 and AerMet 100 steels. At R = 0.9, the three da/dN versus ΔK curves level off, and the level is highest for 4340 steel, intermediate for 300M steel, and lowest for AerMet 100 steel. This observation evidences that the resistance to corrosion fatigue crack growth is greatest for AerMet 100 steel, intermediate for 300M steel, and least for 4340 steel in 3.5% NaCl solution.

VARIATION OF FATIGUE CRACK GROWTH/TIME, da/dt, WITH MAXIMUM STRESS INTENSITY, K_{max}

For the fatigue test in 3.5% NaCl solution, the fatigue crack growth per cycle, da/dN, was converted to the corresponding crack growth per unit time, da/dt, following the relationship da/dt

= f(da/dN), where f is the loading frequency. The da/dt is plotted against the maximum stress intensity, K_{max}, in figure A-6. Also, the SCC growth rate, da/dt, in 3.5% NaCl is plotted against the applied stress intensity, K_I, in this figure. [The SCC plots of 300M and 4340 steels were determined in this study and that of AerMet 100 steel by Oehlert and Atrens (reference 7).]

The upper portion of the da/dt versus K_{max} curve is in the region of $K_{max} > K_{ISCC}$, more at R = 0.9 than at R = 0.1.

FRACTOGRAPHIC FEATURES

The following fractographic features are observable for the three steels.

AERMET 100 STEEL

Figure A-7 shows the da/dN versus ΔK curves and the Scanning Electron Microscope (SEM) fractographs of AerMet 100 steel, fatigue-tested in vacuum. At R = 0.1, cleavagelike facets and scattered dimples are seen. With increasing da/dN, the cleavagelike facets become larger, and striations are visible on the cleavagelike facets. At R = 0.9, mixture of cleavagelike facets and dimples are visible at low da/dN, the number and size of dimple increase with increasing da/dN, and the crack surface is mostly covered by dimples at high da/dN.

Figure A-8 shows a series of changes in SEM fractograph with increasing da/dN for AerMet 100 steel, fatigue-tested at R = 0.1 in vacuum. Cleavagelike facets grow and striations on the facets are more clearly visible with increasing da/dN.

Figure A-9 shows the da/dN versus ΔK curves and the SEM fractographs of AerMet 100 steel, fatigue-tested in air. The fractographic features are similar to those of AerMet 100 steel, fatigue-tested in vacuum.

Figure A-10 shows the da/dt versus K_{max} and K_I curves and the SEM fractographs of AerMet 100 steel, fatigue- and SCC-tested in 3.5% NaCl solution. At R = 0.1 and $K_{max} < K_{ISCC}$, cleavagelike facets and some dimples are seen at low da/dt. With increasing da/dt, the cleavagelike facet becomes larger. At R = 0.9 and low da/dt, mixed cleavagelike and intergranular facets are visible, whereas at high da/dt, mostly dimples are seen. At the initial stage of SCC, mixed cleavagelike and intergranular facets, secondary cracks, and some dimples are noticeable. At the later stage of SCC, intergranular facets, secondary cracks, and dimples are visible. Figure A-11 shows a series of changes in SEM fractograph with increasing da/dN for AerMet 100 steel, fatigue-tested at R = 0.9 in 3.5% NaCl solution. At low da/dN, mixed cleavagelike and intergranular facets are visible, striations on the facets and secondary cracks along facet-boundaries become more noticeable with increasing da/dN, and dimples cover the crack surface at high da/dN.

300M STEEL

Figure A-12 shows the da/dN versus ΔK curves and the SEM fractographs of 300M steel, fatigue-tested in vacuum. At $R = 0.1$, cleavagelike facets and dimples are seen at low da/dN. With increasing da/dN, the cleavagelike facets become larger and dimples become more numerous. At high da/dN, the crack surface is mostly covered by dimples. At $R = 0.9$, mixture of large and disintegrating cleavagelike facets and dimples are visible at low da/dN, and the crack surface is completely covered by dimples at high da/dN.

Figure A-13 shows the da/dN versus ΔK curves and the SEM fractographs of 300M steel, fatigue-tested in air. At $R = 0.1$, cleavagelike facets and dimples are seen at low da/dN. With increasing da/dN, the cleavagelike facets become larger and striations with secondary cracks are visible. At $R = 0.9$, larger cleavagelike facets and dimples are visible at low da/dN, and the cleavagelike facets are disintegrating and replaced by dimples at high da/dN.

Figure A-14 shows the da/dt versus K_{max} and K_I curves and the SEM fractographs of 300M steel, fatigue- and SCC-tested in 3.5% NaCl solution. At $R = 0.1$, cleavagelike facets and some dimples are visible at low da/dt and $K_{max} < K_{ISCC}$, but large cleavagelike facets, striations, secondary cracks, and intergranular facets at higher da/dt and $K_{max} > K_{ISCC}$. At $R = 0.9$, mixed cleavagelike and intergranular facets are visible at low da/dt and $K_{max} < K_{ISCC}$ and mostly intergranular facets and secondary cracks along the facet boundaries at higher da/dt and $K_{max} > K_{ISCC}$. At the initial stage of SCC, intergranular facets and secondary cracks are mostly seen. At the later stage of SCC, intergranular facets, secondary cracks, and dimples are visible.

4340 STEEL

Figure A-15 shows the da/dN versus ΔK curves and the SEM fractographs of 4340 steel, fatigue-tested in vacuum. The fractographic features are mostly similar to those of 300M steel, fatigue-tested in vacuum.

Figure A-16 shows the da/dN versus ΔK curves and the SEM fractographs of 4340 steel, fatigue-tested in air. The fractographic features are similar to those of 300M steel, fatigue-tested in air.

Figure A-17 shows the da/dt versus K_{max} and K_I curves and the SEM fractographs of 4340 steel, fatigue- and SCC-tested in 3.5% NaCl solution. At $R = 0.1$, mostly intergranular facets and patches of dimples are seen at low and high da/dt and K_{max} below and above the K_{ISCC}. More dimples are visible at greater da/dt. At $R = 0.9$, intergranular facets and secondary cracks are mostly seen at low and high da/dt. At the initial stage of SCC, only intergranular facets and secondary cracks are seen. At the later stage of SCC, intergranular facets, secondary cracks, and dimples are visible.

DISCUSSION

STRESS RATIO EFFECT

It was observed that da/dN increased and ΔK_{th} decreased with increasing stress ratio from 0.1 to 0.9 in the three environments for the three steels. This observation is similar to those for various steels and alloys reported by a number of investigators (references 8 through 22).

ENVIRONMENTAL EFFECT

Compared to air, 3.5% NaCl solution enhanced the fatigue crack growth in AerMet 100 steel at $R = 0.9$ but retarded it at $R = 0.1$ in the near-threshold crack growth regime, figure A-4. Similar observations were reported for 2 ¼ Cr-1 Mo, rotor, and 4340 steels and attributed to oxide-induced crack closure (references 11, 12, 14, 23, 24). But such a crack growth retardation by 3.5% NaCl solution was not observed for 300M and 4340 steels at $R = 0.1$.

As figure A-6 shows, the lower portion of the da/dt versus K_{max} curve for the fatigue test at $R = 0.1$ in 3.5% NaCl solution is in the region of $K_{max} < K_{ISCC}$, and no SCC is expected to occur under cyclic loading in this region. Yet the 3.5% NaCl solution can still influence the fatigue crack growth process and induce the true or environmental corrosion fatigue (reference 25). On the other hand, in the region of $K_{max} > K_{ISCC}$, the stress corrosion crack growth is superimposed over the fatigue crack growth, resulting in stress corrosion fatigue (reference 25). The SCC contribution to fatigue crack growth has also been discussed by the other investigators (references 26 through 29).

Wei and Landes (reference 26) considered the fatigue crack growth in high-strength steels in an aggressive environment to be composed of two components, mechanical and environmental. They proposed that the da/dN in an aggressive environment, $(da/dN)_c$, could be expressed in terms of the da/dN in an inert reference environment, $(da/dN)_r$, and an environment component computed from sustained-load crack growth data. Gerberich, Birat, and Zackay (reference 27) proposed that the da/dN in a corrosive environment consisted of a fatigue contribution, $(da/dN)_f$, and a SCC contribution, $(da/dN)_{SCC}$. Wei (reference 26) redefined his previous model as the da/dN in an aggressive environment, $(da/dN)_e$, composing of three components, $(da/dN)_r$ for pure fatigue in inert or reference environment, $(da/dN)_{cf}$ for environmental contribution due to the synergistic interaction of fatigue and environmental attack, and $(da/dN)_{SCC}$ for SCC at $K > K_{ISCC}$. Pao, Wei, and Wei (reference 29) studied the fatigue crack growth behavior of 4340 steel in water vapor and pointed out the environmental contribution arising from SCC for $K_{max} > K_{ISCC}$ and from synergistic action of fatigue and environmental attack for $K_{max} < K_{ISCC}$.

FRACTOGRAPHIC FEATURES

In vacuum and air, at $R = 0.1$, the fractographic features are similar for the three steels, cleavagelike facets at lower da/dN and enlarged cleavagelike facets and some dimples at higher da/dN. At $R = 0.9$, the number and size of dimple increase with increasing da/dN. This observation evidences that, in vacuum and air.

- The cleavagelike facet is enlarged with increasing da/dN and R.
- The number and size of dimple increase with increasing da/dN and R.
- The enlarged cleavagelike facets are disintegrated and replaced by dimples at higher da/dN and R.

In 3.5% NaCl solution, at R = 0.1, cleavagelike facets and some dimples are seen at lower da/dN (or da/dt) and enlarged cleavagelike facets at higher da/dN for the AerMet 100 steel. However, at R = 0.9, mixed cleavagelike and intergranular facets are visible at lower da/dN and mostly dimples at higher da/dN. More intergranular facets are present at higher da/dN and R = 0.1, and mixed cleavagelike and intergranular facets at lower da/dN and mostly intergranular facets at higher da/dN for the 300M steels. On the other hand, mostly intergranluar facets are present at low and high da/dN and R = 0.1 and 0.9 for the 4340 steel. This observation evidences that, in 3.5% NaCl solution.

- Cleavagelike facets and dimples are still seen at lower R and da/dN in more corrosion fatigue resistant steel, such as the AerMet 100 steel. However, these fractographic features are replaced by mixed cleavagelike and intergranular facets at higher R and lower da/dN, and they are mostly replaced by dimples at higher da/dN.
- In lower corrosion fatigue resistance steels, such as the 300M and 4340 steels, more intergranular facets cover the crack surface at low and high da/dN and R.

At the beginning of SCC in 3.5% NaCl solution, the fractographic features are predominantly intergranular facets for the three steels. At the later stage of SCC, intergranular facets, secondary cracks, and dimples are visible.

These observations indicate that the susceptibility to intergranular cracking or grain boundary decohesion is greatest for the 4340 steel, somewhat less for the 300M steel, and least for the AerMet 100 steel during fatigue and SCC in 3.5% NaCl solution. Considering the relative values of K_{ISCC} of the three steels, the least for 4340 steel, slightly greater for 300M steel, and the greatest for AerMet 100 steel, the greater susceptibility to intergranular cracking corresponds to smaller K_{ISCC} or smaller SCC resistance.

GRAIN SIZE EFFECT

It has been known that, in the near-threshold regime of fatigue crack growth, an increase in the grain size generally results in a marked reduction in da/dN and an increase in ΔK_{th} (reference 6). However, such a grain size effect on fatigue crack growth is not noticeable in this study, especially in 3.5% NaCl solution. As figure A-5 shows, the AerMet 100 steel has the lowest da/dN and the greatest ΔK_{th} in 3.5% NaCl solution, though it has the smallest grain diameter of prior austenite (6 μm), compared to those (20 and 14 μm) of the 300M and 4340 steels. Apparently, the higher inherent resistance of the AerMet 100 steel to corrosion fatigue crack growth overwhelms the unfavorable grain size effect.

THIS PAGE INTENTIONALLY LEFT BLANK

CONCLUSIONS

- da/dN increases and ΔK_{th} decreases with increasing R in vacuum, air, and 3.5% NaCl solution.
- Crack growth is retarded at R = 0.1 in the near-threshold regime for the AerMet 100 steel in 3.5% NaCl solution. This is attributable to corrosion product induced crack closure.
- The main fractographic features of fatigue in vacuum and air are cleavagelike facets and some dimples at lower da/dN and R. The cleavagelike facets are enlarged, disintegrated, and replaced by increasing number of dimples with increasing da/dN and R.
- The key fractographic features of fatigue in 3.5% NaCl solution are mixed cleavagelike and intergranular facets at lower da/dN and R for the AerMet 100 steel. On the other hand, intergranular facets and secondary cracks are predominant features for the fatigue of the 300M and 4340 steels in 3.5% NaCl solution. These fractographic features of fatigue are similar to those of SCC in 3.5% NaCl solution.
- Resistance to fatigue and intergranular cracking in 3.5% NaCl solution is greatest for the AerMet 100 steel, intermediate for the 300M steel, and least for the 4340 steel.

THIS PAGE INTENTIONALLY LEFT BLANK

REFERENCES

1. Little, Clayton D. and Machmeier, Paul M., "High Strength Fracture Resistant Weldable Steels," *U. S. Patent No. 4,076,525,* Feb. 28, 1978.

2. Hemphill, Reymond M. and Wert, David E., "High Strength, High Fracture Toughness Structural Alloy," *U.S. Patent No. 5,087,415,* Feb. 11, 1992.

3. Saxena, Ashok and Hudak, S. J., Jr., "Review and Extension of Compliance Information for Common Crack Growth Specimens," *International Journal of Fracture,"* Vol. 14, 1978, pp. 453-468.

4. ASTM Standard E 399 –90, "Standard Test Method for Plane-Strain Fracture Toughness of Metallic Materials," *2003 Annual Book of ASTM Standards,* Vol. 03.01, pp. 451-482.

5. Murakami, Y., "Single Edge Cracked Pure Bending Specimen (SEB)," *Stress Intensity Factors Handbook,* Vol. 1, Pergamon Press, New York, NY, 1987, pp. 11-12.

6. Suresh, S., *Fatigue of Materials,* Cambridge University Press, Cambridge, UK, 1991, p. 203 and 211.

7. Oehlert, A. and Atrens, A., "Stress Corrosion Crack Propagation in AerMet 100," *Journal of Materials Science,* Vol. 33, 1998, pp. 775-781.

8. Schmidt, R. A. and Paris, P. C., "Threshold for Fatigue Crack Propagation and the Effects of Load Ratio and Frequency," *Progress in Flaw Growth and Fracture Toughness Testing, ASTM STP 536,* American Society for Testing and Materials, 1973, pp. 79-94.

9. Kirby, B. R. and Beevers, C. J., "Slow Fatigue Crack Growth and Threshold Behaviour in Air and Vacuum of Commercial Aluminum Alloys," *Fatigue of Engineering Materials and Structures,* Vol. 1, 1979, pp. 203-215.

10. Ritchie, R. O., "Near-Threshold Fatigue-Crack Propagation in Steels," *International Metals Reviews,* Nos. 5 and 6, 1979, pp. 205-230.

11. Stewart, A. T., "The Influence of Environment and Stress Ratio on Fatigue Crack Growth at Near Threshold Stress Intensities in Low-Alloy Steels," *Engineering Fracture Mechanics,* Vol. 13, 1980, pp. 463-478.

12. Ritchie, R. O., Suresh, S., and Moss, C. M., "Near-Threshold Fatigue Crack Growth in 2 ¼ Cr-1 Mo Pressure Vessel Steel in Air and Hydrogen," *Journal of Engineering Materials and Technology,* Vol. 102, 1980, pp. 293-299.

13. Nakai, Y., Tanaka, K., and Nakanishi, T., "The Effects of Stress Ratio and Grain Size on Near-Threshold Fatigue Crack Propagation in Low-Carbon Steel," *Engineering Fracture Mechanics*, Vol. 15, 1981, pp. 291-302.

14. Suresh, S., Zamiski, G. F., and Ritchie, R. O., "Oxide-Induced Crack Closure: An Explanation for Near-Threshold Corrosion Fatigue Crack Growth Behavior," *Metall Trans A*, Vol. 12A, 1981, pp. 1435-1443.

15. Lafarie-Frenot, M. C. and Gasc, C., "The Influence of Age-Hardening on Fatigue Crack Propagation Behaviour in 7075 Aluminum Alloy in Vacuum," *Fatigue of Engineering Materials and Structures*, Vol. 6, 1983, pp. 329-344.

16. Gray, G. T., III., Williams, J. C., and Thompson, A. W., "Roughness-Induced Crack Closure: An Explanation for Microstructurally Sensitive Fatigue Crack Growth," *Metall Trans A*, Vol. 14A, 1983, pp.421-433.

17. Doker, H. and Marci, G., "Threshold Range and Opening Stress Intensity Factor in Fatigue," *International Journal of Fatigue*, Vol. 5, 1983, pp. 187-191.

18. Suresh, S., Vasudevan, A. K., and Bretz, P. E., "Mechanisms of Slow Fatigue Crack Growth in High Strength Aluminum Alloys: Role of Microstructure and Environment, *Metall. Trans. A*, Vol. 15A, 1984, pp. 369-379.

19. Liaw, P. K., Saxena, A., Swaminathan, V. P., and Shin, T. T., "Influence of Temperature and Load Ratio on Near-Threshold Fatigue Crack Growth Behavior of CrMoV Steel," *Fatigue Crack Growth Threshold Concepts*, D. L. Davidson and S. Suresh, Eds., The Metallurgical Society of AIME, 1984, pp. 205-223.

20. Blom, A. F., "Near-Threshold Fatigue Crack Growth and Crack Closure in 17-4 PH Steel and 2024-T3 Aluminum Alloy," *ibid*, pp. 263-279.

21. Cadman, A. J., Nicholson, C. E., and Brook, R., "Influence of R Ratio and Orientation on the Fatigue Crack Threshold and Subsequent Crack Growth of a Low-Alloy Steel," *ibid*, pp. 281-298.

22. Esaklul, K. A., Wright, A. G., and Gerberich, W. W., "An Assessment of Internal Hydrogen Versus Closure Effects on Near-Threshold Fatigue Crack Propagation," *Ibid*, pp. 299-326.

23. Liaw, P. K., Leax, T. R., and Donald, J. K., "Fatigue Crack Growth Behavior of 4340 Steels," *Acta Metall*, Vol. 35, 1987, pp. 1415-1432.

24. Tu, L. K. L. and Seth, B. B., "Threshold Corrosion Fatigue Crack Growth in Steels," *Journal of Testing and Evaluation*, Vol. 6, 1978, pp. 66-74.

25. Vasudevan, A. K., Sadananda, K., and Glinka, G., "Critical Parameters for Fatigue Damage," *International Journal of Fatigue*, Vol. 23, 2001, pp. S39-S53.

26. Wei, R. P. and Landes, J. D., "Correlation between Sustained-Load and Fatigue Crack Growth in High-Strength Steels," *Materials Research and Standards,* Vol. 9, 1969, pp. 25-46.

27. Gerberich, W. W., Birat, J. P., and Zackay, V. F., "On the Superposition Model for Environmentally-Assisted Fatigue Crack Propagation," *Corrosion Fatigue: Chemistry, Mechanics and Microstructure, NACE-2,* O. F. Devereux, A. J. McEvily, and R. W. Stehle, Eds., National Association of Corrosion Engineers, 1972, pp. 396-408.

28. Wei, R. P., "On Understanding Environment-Enhanced Fatigue Crack Growth – a Fundamental Approach," *Fatigue Mechanisms, J. T. Fong, Ed., ASTM STP 675,* 1979, pp. 816-840.

29. Pao, P. S., Wei, W., and Wei, R. P., "Effect of Frequency on Fatigue Crack Growth Response of AISI 4340 Steel in Water Vapor," *Environment-Sensitive Fracture of Engineering Materials,* Z. A. Foroulis, Ed., The Metallurgical Society of AIME, 1979, pp. 565-580.

THIS PAGE INTENTIONALLY LEFT BLANK

APPENDIX A
FIGURES

APPENDIX A

4340 Steel

(14μm)

300M Steel

(20μm)

AerMet 100 Steel

(γ grain dia: 6μm)

Figure A-1: Optical Micrographs of Three Steels

19
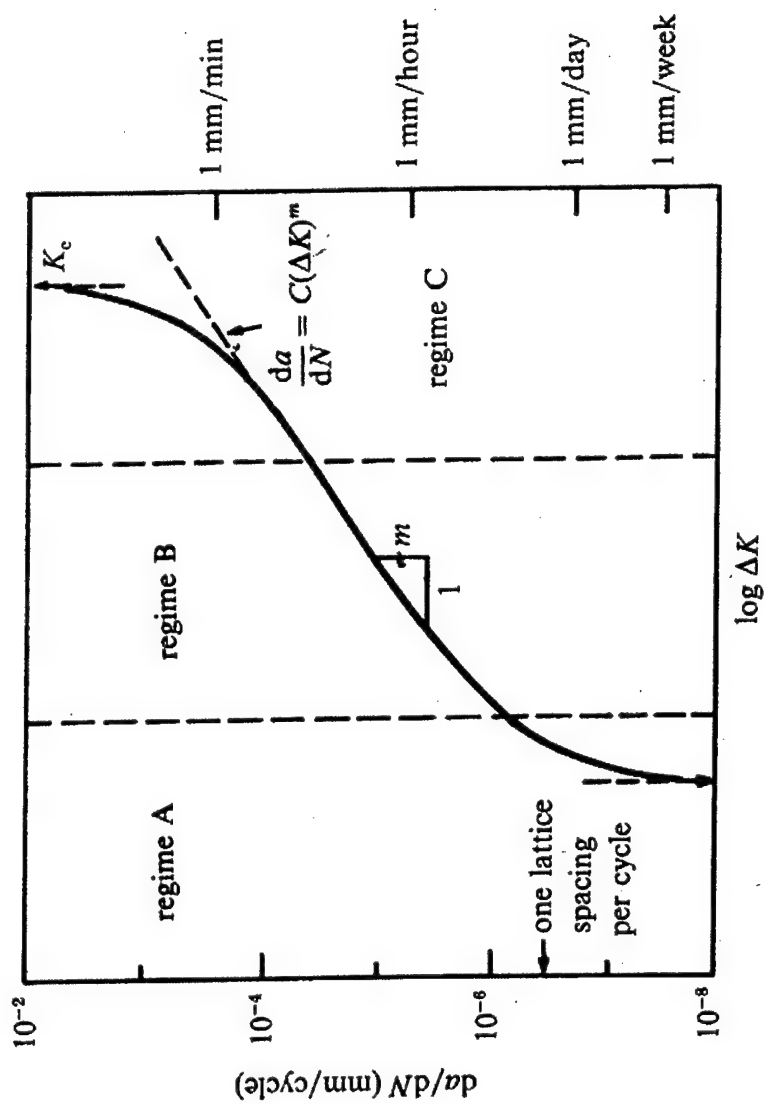
Figure A-2: Schematic Curve of da/dN versus ΔK, Showing Three Regimes of Fatigue Crack Growth
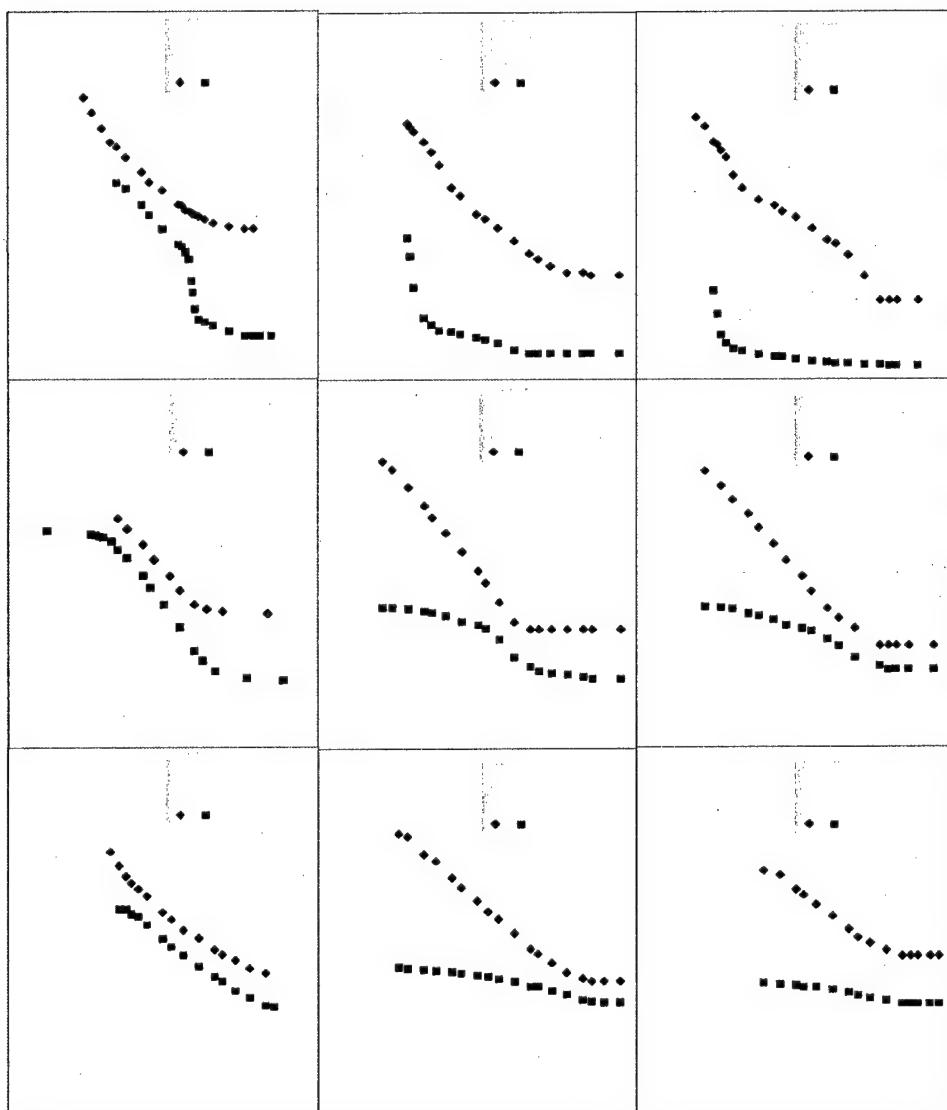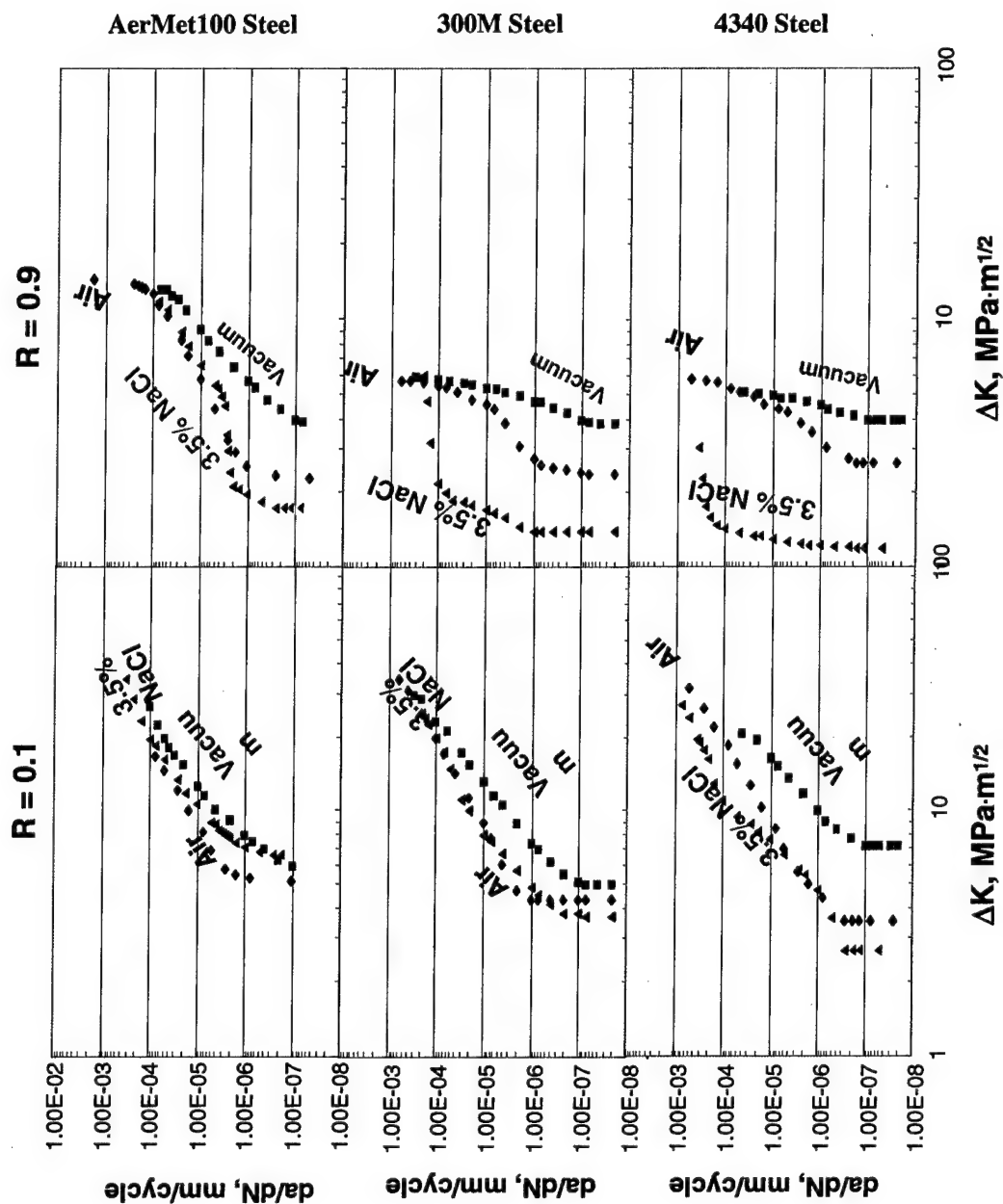
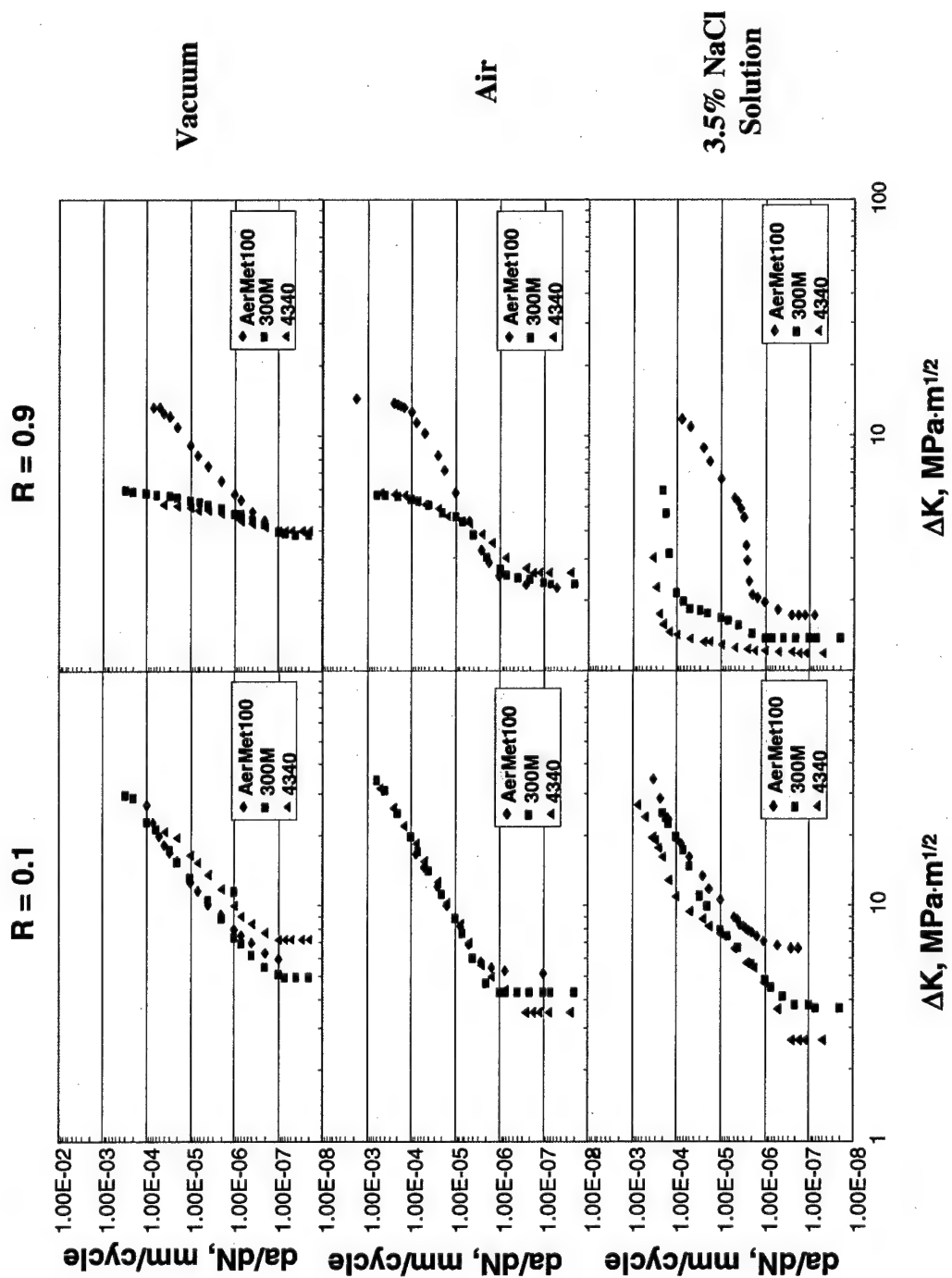Figure A-4: Curves of da/dN versus ΔK, Indicating Environmental Effect

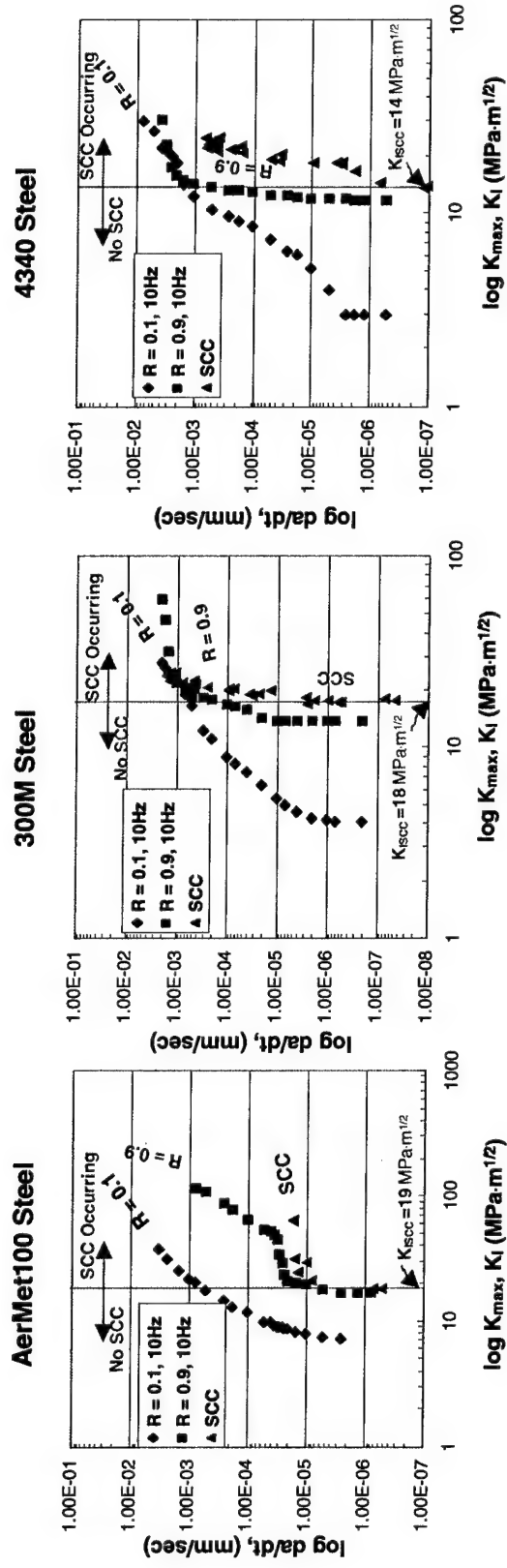Figure A-5: Curves of da/dN versus ΔK, Indicating Relative Fatigue Resistance

23

Figure A-6: Variation of da/dt with K_{max} or K_I
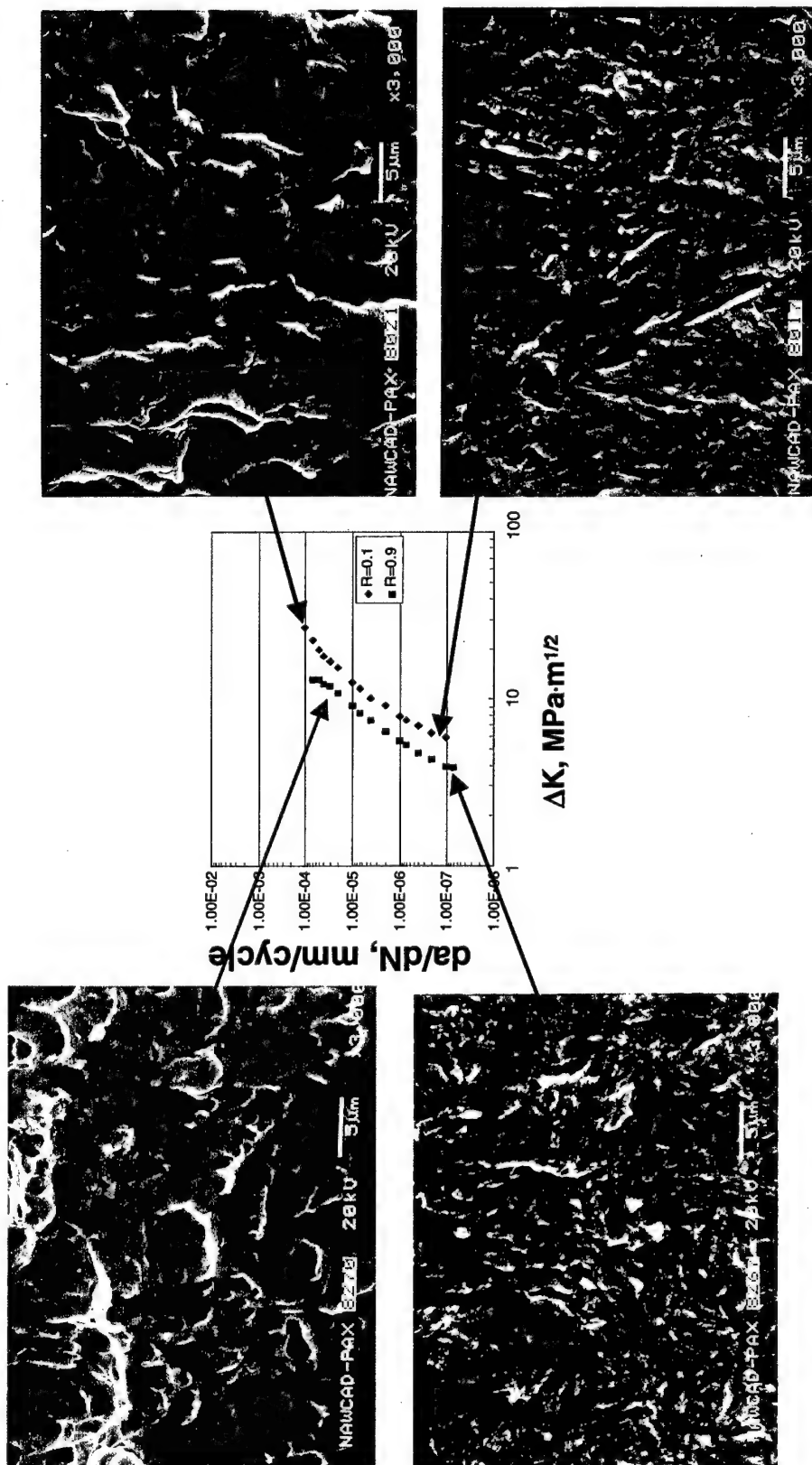
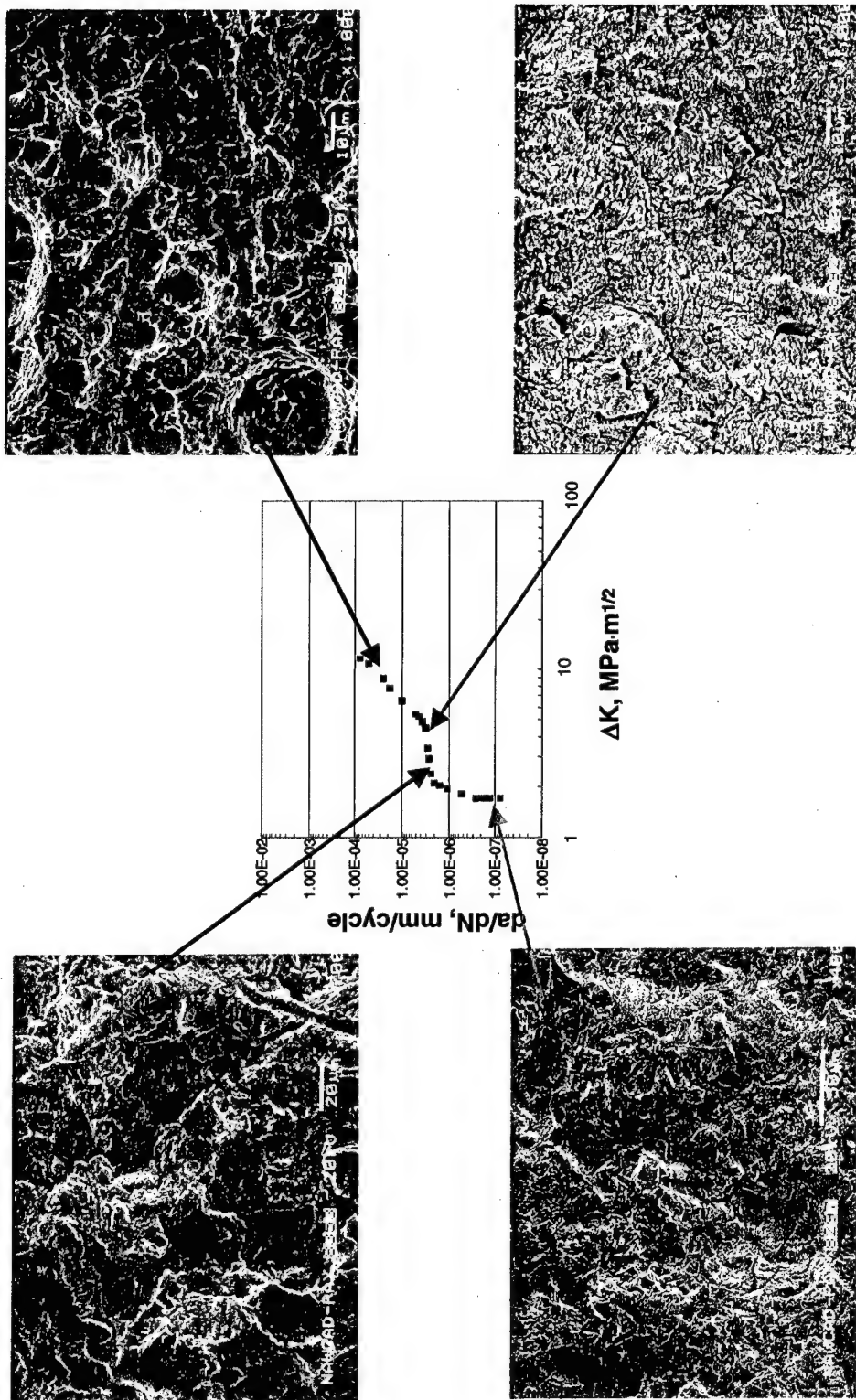Figure A-7: da/dN versus ∆K Curves and SEM Fractographs of AerMet 100 Steel, Fatigue-Tested in Vacuum
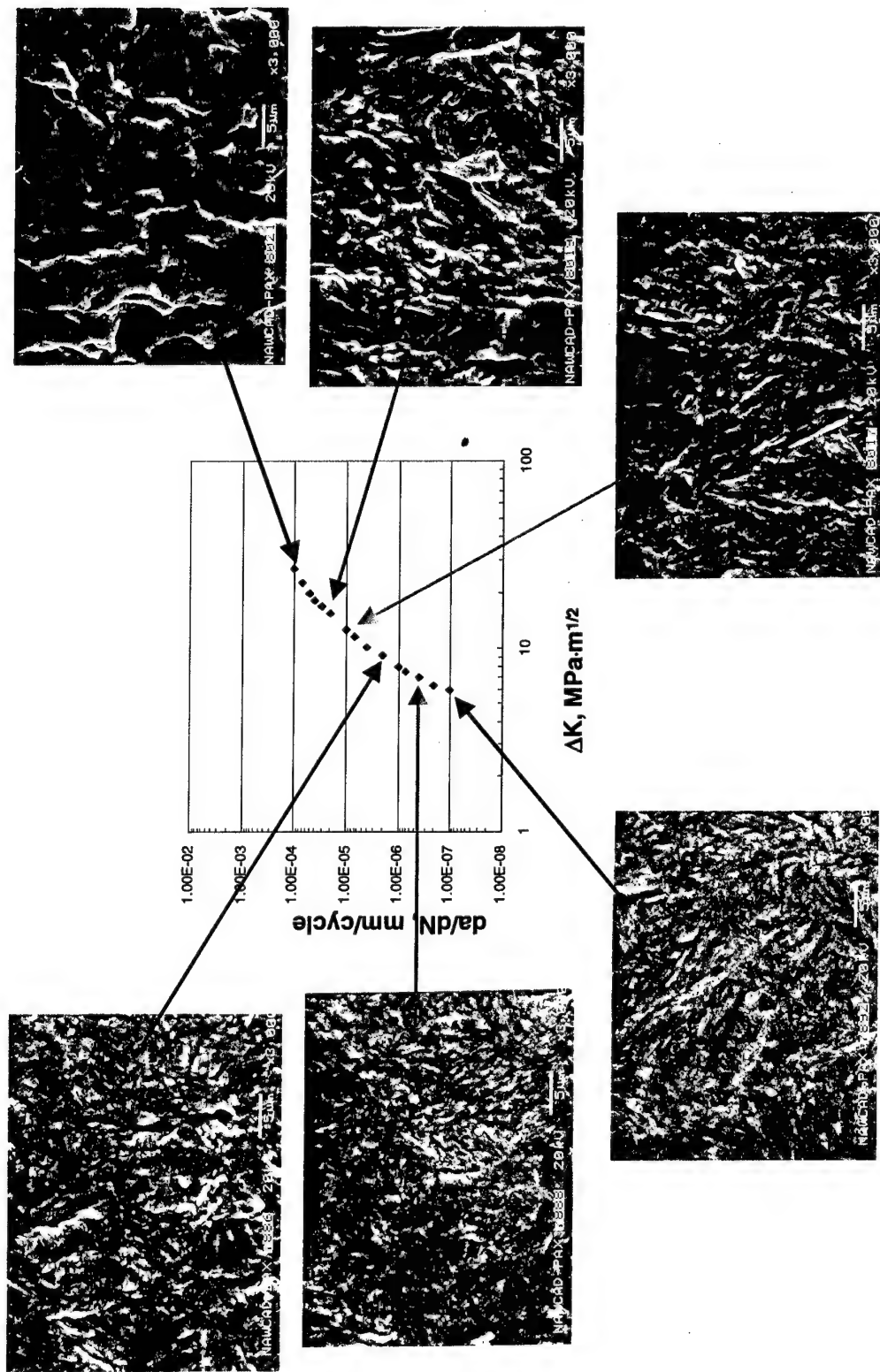
Figure A-8: Detailed Change in SEM Fractographs with Increasing da/dN for AerMet 100 Steel, Fatigue-Tested at R = 0.1 in Air
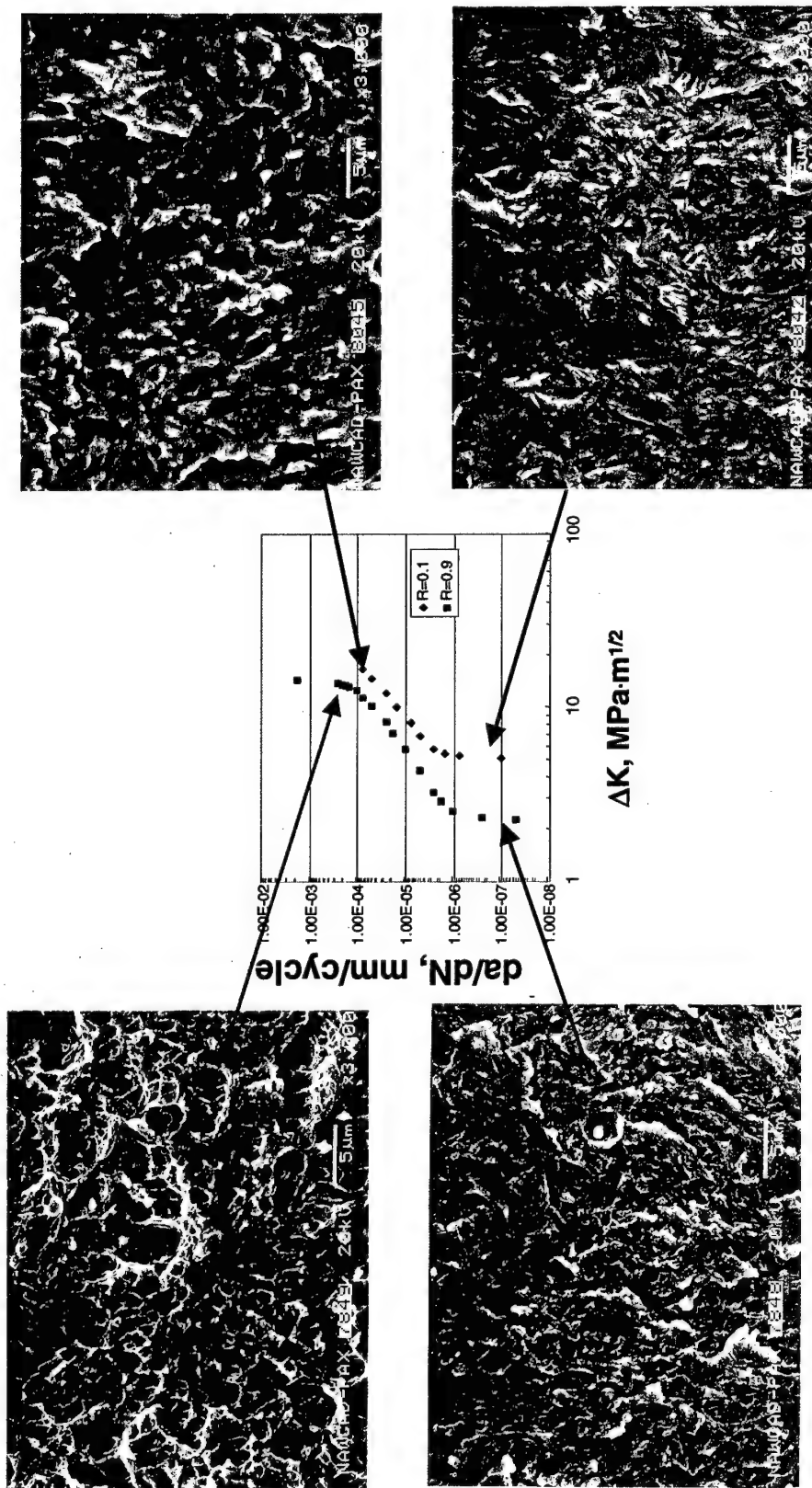
Figure A-9: da/dN versus ΔK Curves and SEM Fractographs of AerMet 100 Steel, Fatigue-Tested in Air
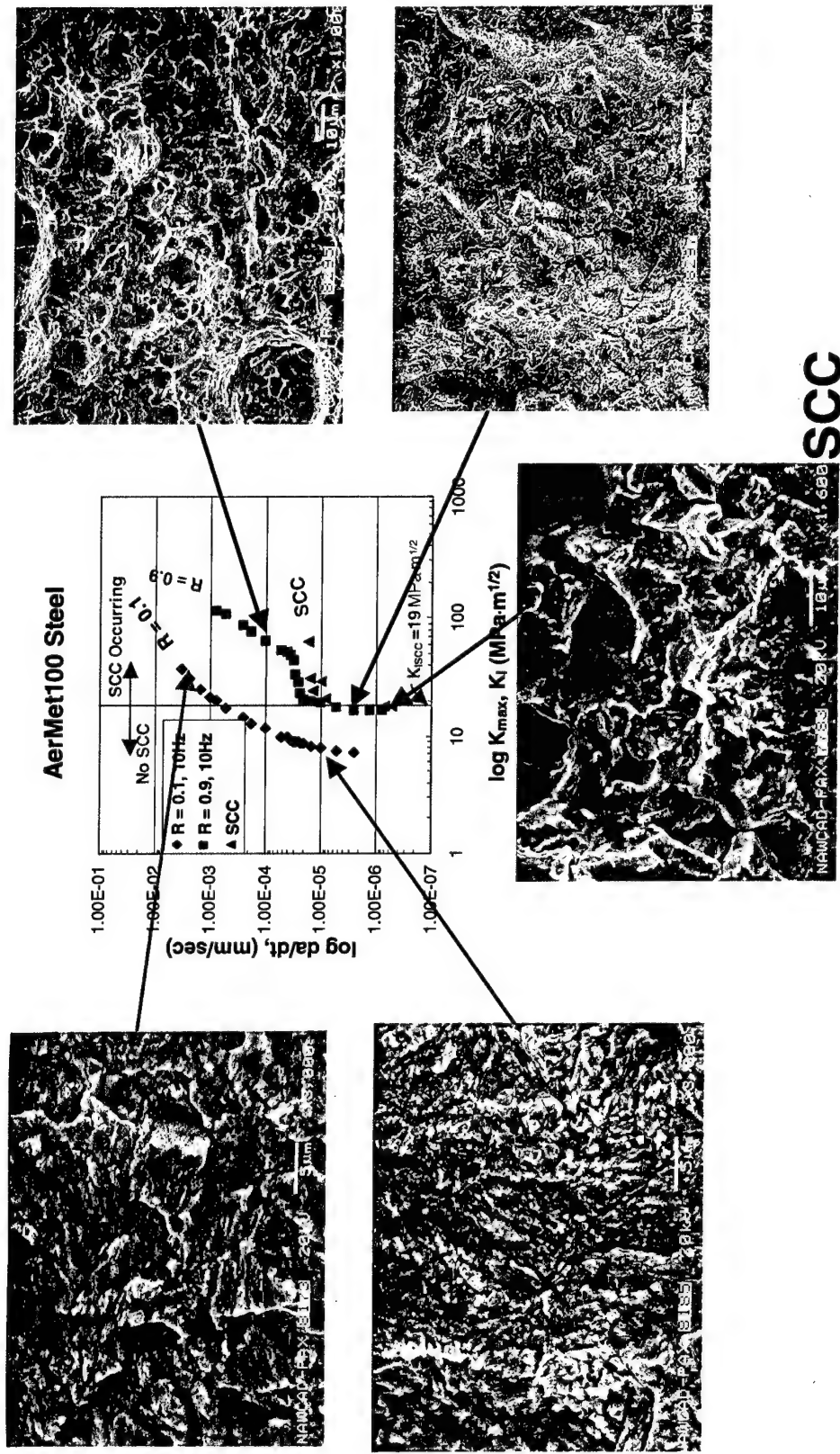
Figure A-10: da/dt versus K_{max} and K_I Curves and SEM Fractographs of AerMet 100 Steel, Fatigue- and SCC-Tested in 3.5% NaCl Solution

Figure A-11: Detailed Change in SEM Fractographs with Increasing da/dN for AerMet 100 Steel, Fatigue-Tested at R = 0.9 in 3.5% NaCl Solution
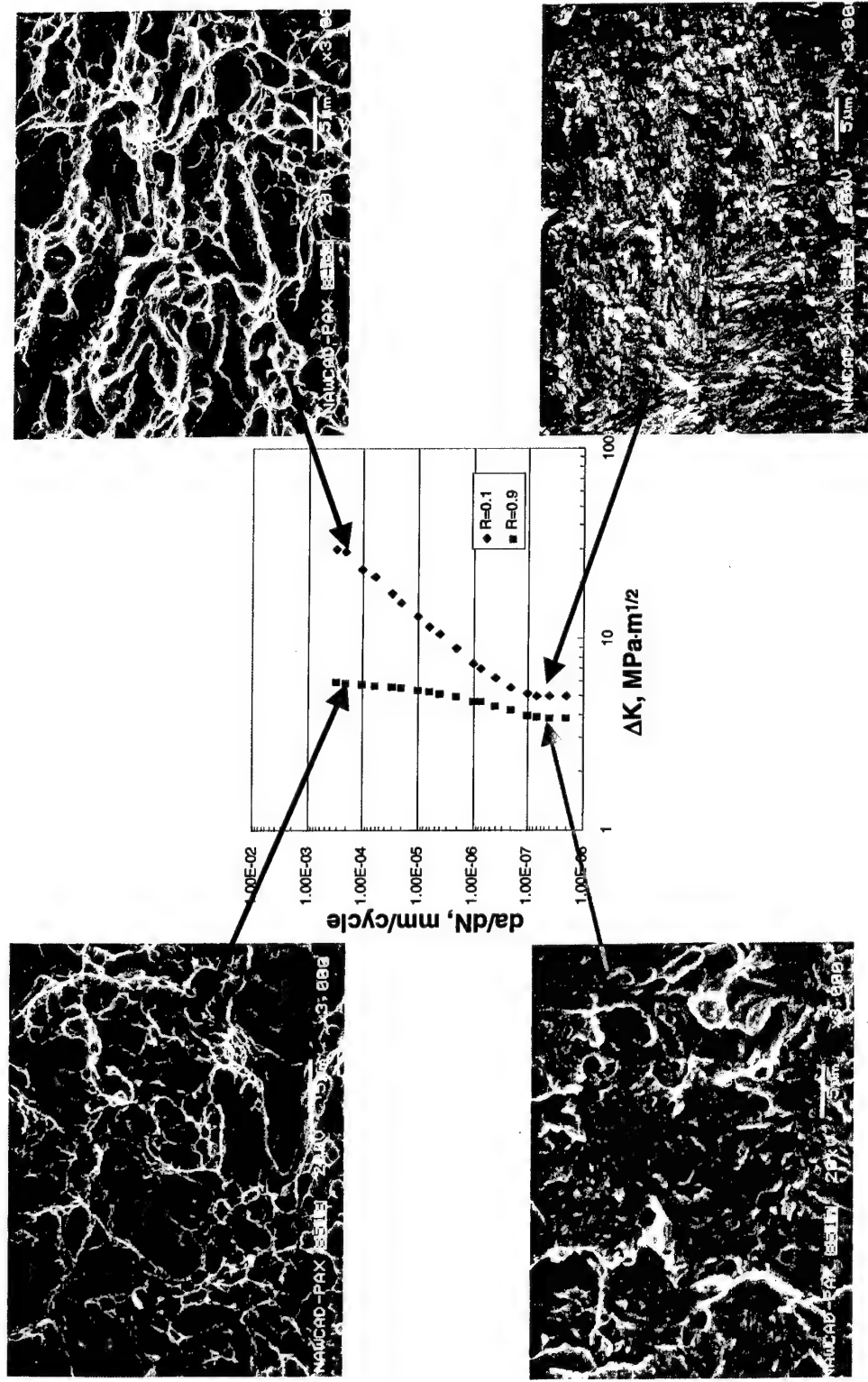
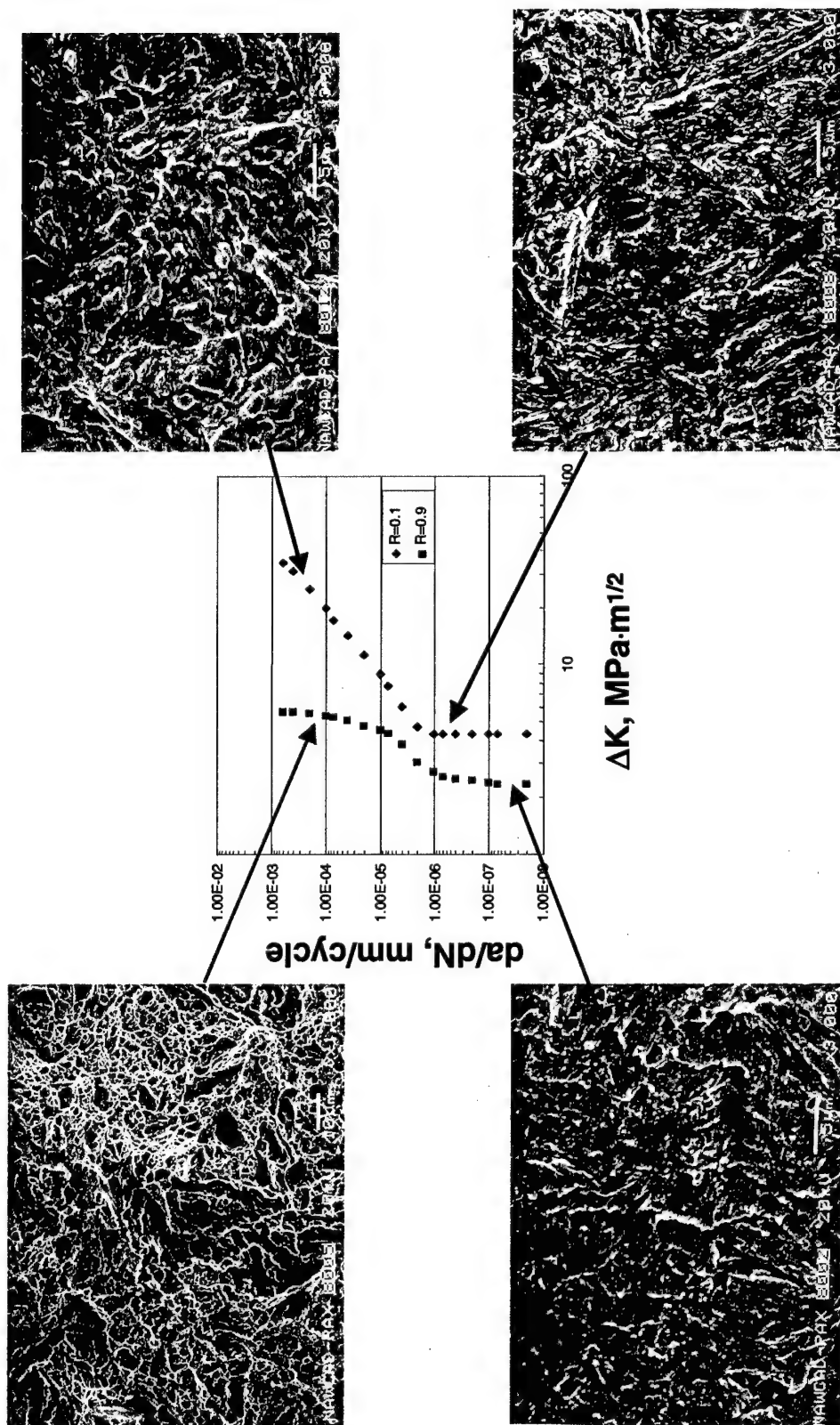Figure A-12: da/dN versus ΔK Curves and SEM Fractographs of 300M Steel, Fatigue-Tested in Vacuum

30

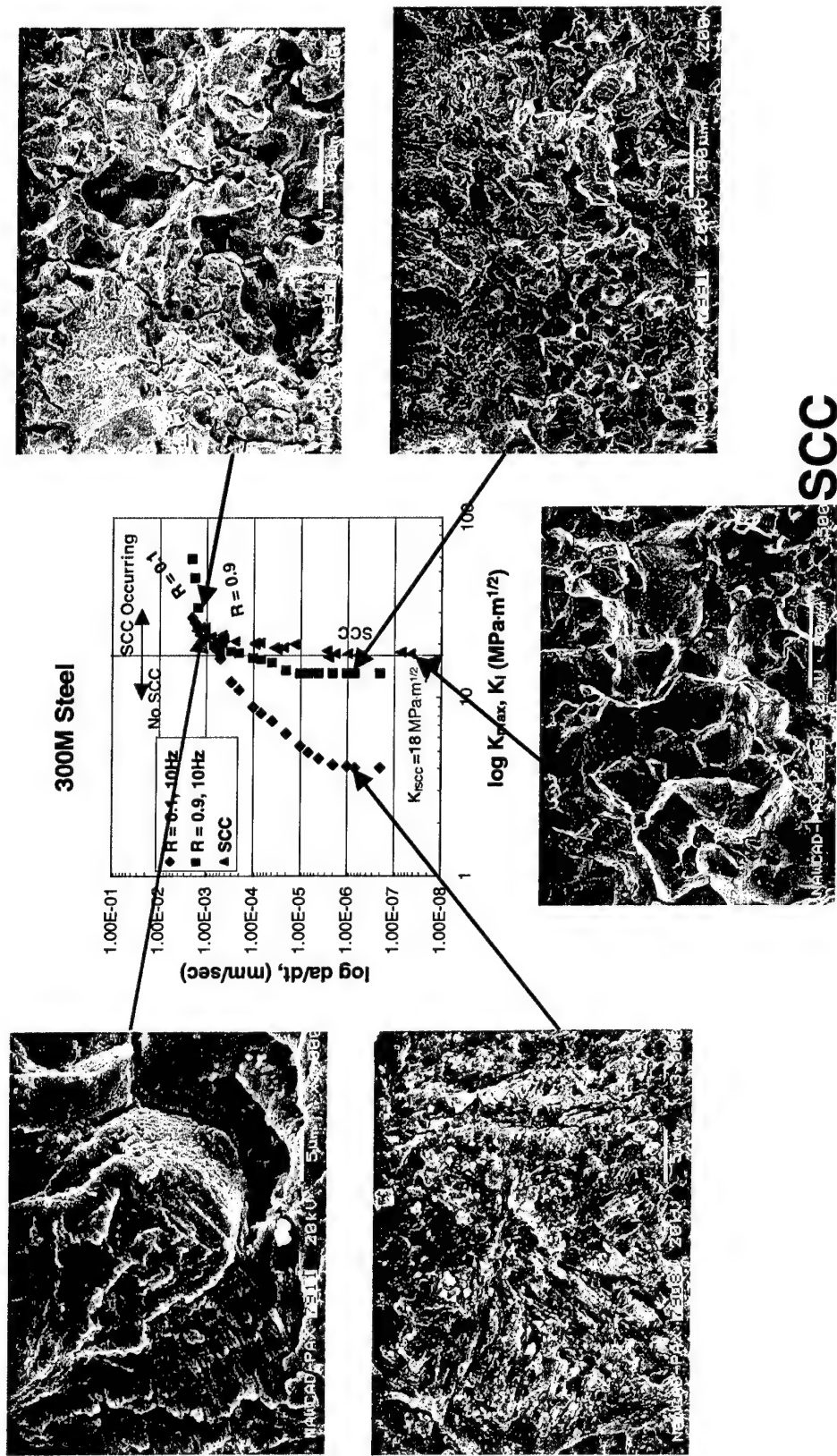Figure A-13: da/dN versus ΔK Curves and SEM Fractographs of 300M Steel, Fatigue-Tested in Air

31

Figure A-14: da/dt versus K_{max} and K_I Curves and SEM Fractographs of 300M Steel, Fatigue- and SCC-Tested in 3.5% NaCl Solution
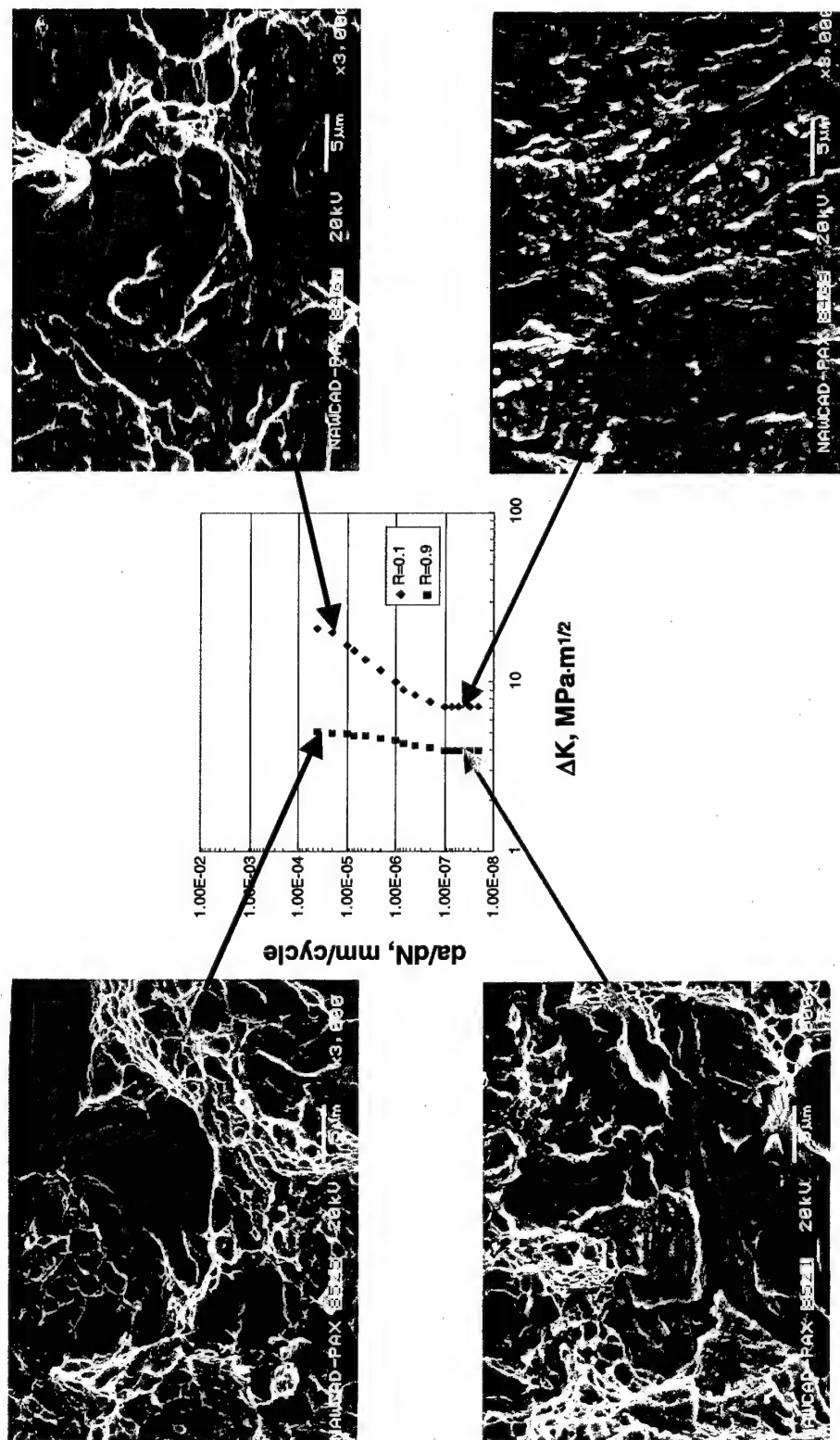
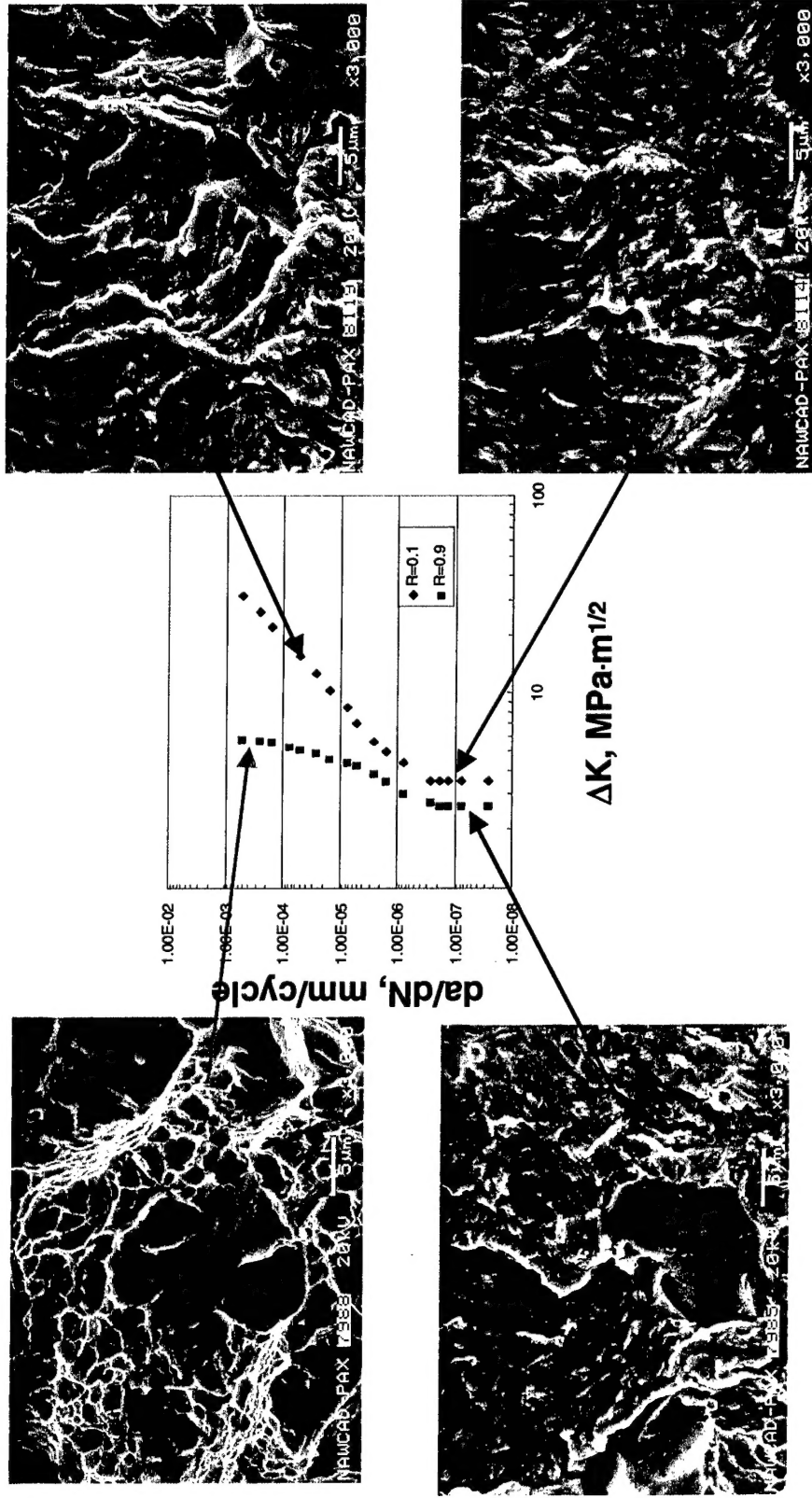Figure A-15: da/dN versus ΔK Curves and SEM Fractographs of 4340 Steel, Fatigue-Tested in Vacuum

33

Figure A-16: da/dN versus ΔK Curves and SEM Fractographs of 4340 Steel, Fatigue-Tested in Air
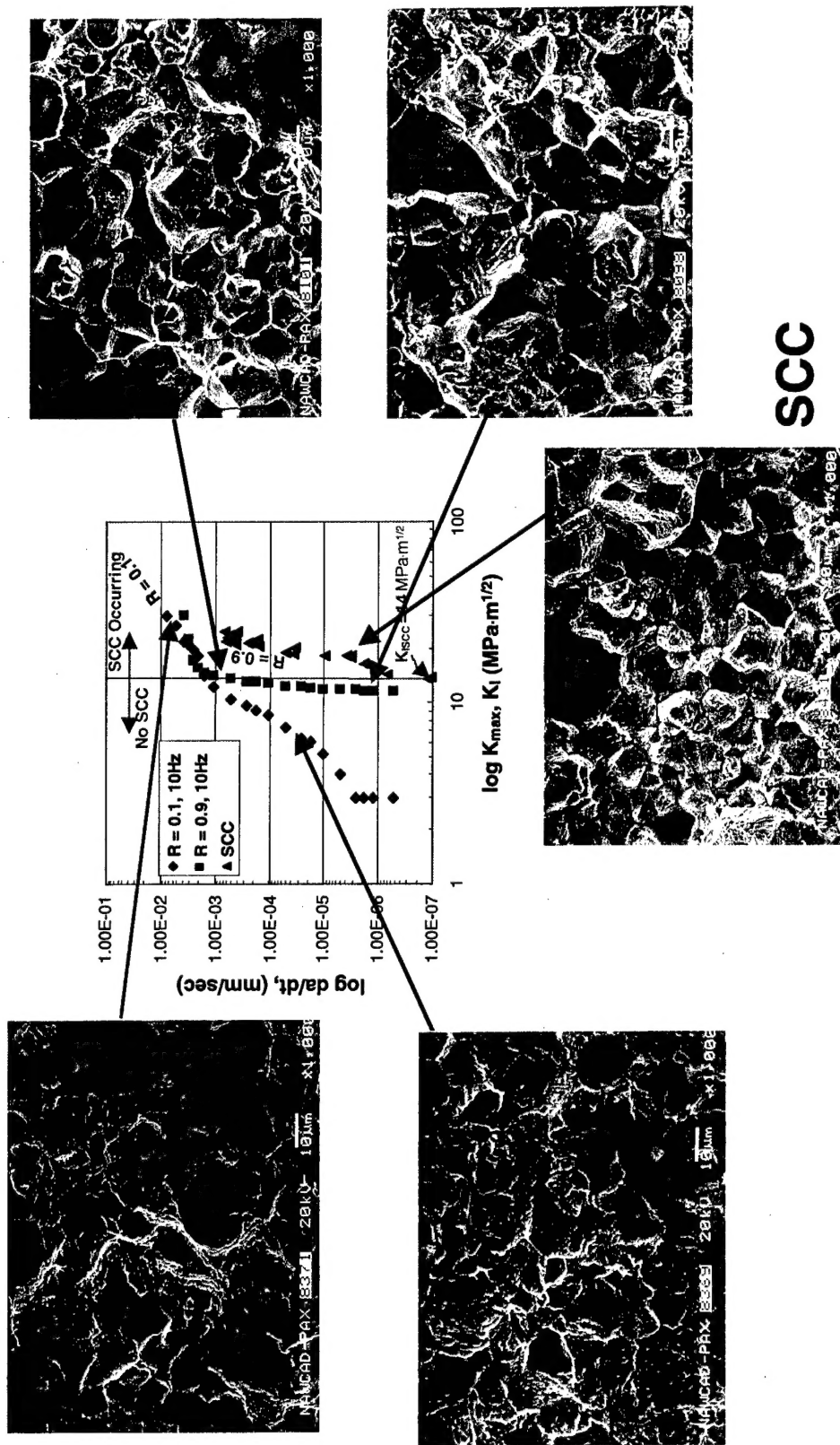
Figure A-17: da/dt versus K_{max} and K_I Curves and SEM Fractographs of 4340 Steel,
Fatigue- and SCC-Tested in 3.5% NaCl Solution

THIS PAGE INTENTIONALLY LEFT BLANK

DISTRIBUTION:

NAVAIRSYSCOM (AIR-5.0E), Bldg. 304, Room 120	(1)
22541 Millstone Road, Patuxent River, MD 20670-1606	
NAVAIRSYSCOM (AIR-4.11), Bldg. 304, Room 102	(1)
22541 Millstone Road, Patuxent River, MD 20670-1606	
NAVAIRSYSCOM (AIR-4.3), Bldg. 2187	(1)
48066 Shaw Road, Patuxent River, MD 20670-1908	
NAVAIRSYSCOM (AIR-4.3.4), Bldg. 2188	(1)
48066 Shaw Road, Patuxent River, MD 20670-1908	
NAVAIRWARCENACDIV (4.3.4.2), Bldg 2188	(50)
48066 Shaw Road, Patuxent River, MD 20670-1908	
NAVAIRWARCENACDIV (7.2.5.1), Bldg. 405, Room 108	(1)
22133 Arnold Circle, Patuxent River, MD 20670-1551	
NAVTESTWINGLANT (55TW01A), Bldg. 304, Room 200	(1)
22541 Millstone Road, Patuxent River, MD 20670-1606	
NAVAIRSYSCOM Aging Aircraft IPT, Bldg. 2185	(1)
22347 Cedar Point Road, Patuxent River, MD 29670-1161	
NAVSEASYSCOM	(1)
2531 Jefferson Davis Highway, Arlington, VA 22242	
Naval Research Laboratory	(1)
4555 Overlook Avenue, S. W., Washington, DC 20375-5000	
NADEP (Code 4.3.4)	(1)
Naval Air Station, Jacksonville, FL 32212	
NADEP (Code 4.3.4)	(1)
222 East Avenue, San Diego, CA 92135-5112	
NADEP (Code 4.3.4)	(1)
Cherry Point, NC 28533	
NAVAIRWARCENACDIV Lakehurst	(1)
Lakehurst, NJ 08733-5000	
Army Materials Command (AMCCE-BD)	(1)
5001 Eisenhower Ave., Alexandria, VA 22333	
DTIC	(1)
8725 John J. Kingman Road, Suite 0944, Ft. Belvoir, VA 22060-6218	